

A numerical investigation of the influence of hydraulic parameters on the stability of a residual soil slope

Jorge Henrique Ribeiro Lins^{1#} , Francisco Chagas da Silva Filho¹ 

Article

Keywords

SWCC
Hysteresis
Soil conductivity
Rainfall
Slope stability

Abstract

The residual tropical soils and their unsaturated condition add more complexity to the study of slope stability, introducing the suction variable to the stress state analysis. Due to the complexity of the pedological processes involved in their formation, tropical soils present variability in their parameters. This results in uncertainties regarding its behaviour in geotechnical structures. The most common promotion agent for deformation and loss of strength in residual soils in an unsaturated condition is the advancing of the wetting front due to rainfalls. A tropical climate with high levels of rainfall makes landslides a constant and dangerous phenomenon, leading to loss of human life and material. Thus, it is essential to verify the influence of precipitation on slope behaviour in residual conditions. This study analyzes the behaviour of a slope formed by a residual soil by determining the soil properties followed by a numerical analysis. Laboratory tests were performed to characterize the soil and determine the strength, hydraulic, and unsaturated condition parameters. In the numerical analysis, it was intended to visualize the influence of rainfall and hydraulic parameters on the pore pressure distribution inside the slope and in its stability. After the numerical step, it was found that the different rainfall characteristics (intensity and duration) increased the pore pressures and decreased the strength of the material. However, it was insufficient to trigger any failure mechanisms. The hydraulic parameters' critical roles at seepage through the soil and how this is reflected in the calculations of safety factors were verified.

1. Introduction

Studying infiltration in residual soil slopes can be a complex task, as it is controlled by factors of different natures. According to Wesley (1990), relating to its formation, residual soils have their main characteristics resulting directly from the chemical and physical in situ processes experienced by the parent rock, resulting in a high level of heterogeneity. Applying its properties in a numerical analysis encounters difficulties linked to the complexity and variability of the material characteristics. For example, different degrees of weathering can be found with increasing depth, each corresponding to a different mechanical and hydrological behaviour (Rahardjo et al., 2012).

In general, soils of this nature are found in an unsaturated condition, subjected to negative pore water pressures that fluctuate as a function of hydrometeorological agents, such as rainfall events. Material parameters required for an unsaturated approach are dependent on moisture path (wetting or drying), stress level and history, in addition to the soil-forming process itself, for example. Regarding rainfall events, their relationship between intensity and duration can produce different soil responses to the infiltration regime.

The most important parameter for an unsaturated approach is the soil-water characteristic curve (SWCC), which can be understood as the relationship between the mass of water in the pores and the energy required for its removal (Carvalho et al., 2015). The measurement of the amount of water can be in the form of the degree of saturation (S), volumetric water content (θ) or gravimetric water content (w) (Kristo et al., 2019). Soil structure and capillarity are the primary characteristics of water retention at low suction values. At higher values, mineralogy and the specific surface of the particles are protagonists. The SWCC can be obtained through two paths: adsorption/wetting and desorption/drying. At a given suction, the soil moisture on a drying curve is higher than on a wetting curve. This phenomenon is known as hydraulic hysteresis. Wetting and drying correspond to the curves of a wetting curve from a dry state and a drying curve from a saturated state, respectively (Lai, 2004).

There is a strong motivation for understanding of hysteresis in SWCC and its impact on stress, shear strength, flow, and deformation behaviours of unsaturated soils. Infiltration of rainwater (or snow melting) and evapotranspiration promote cyclical processes of wetting and drying in soils.

[#]Corresponding author. E-mail address: jorgerlins14@gmail.com

¹Universidade Federal do Ceará, Departamento de Hidráulica e Engenharia Ambiental, Fortaleza, CE, Brasil.

Submitted on November 22, 2022; Final Acceptance on February 19, 2024; Discussion open until May 31, 2024.

<https://doi.org/10.28927/SR.2024.012022>



This is an Open Access article distributed under the terms of the Creative Commons Attribution License, which permits unrestricted use, distribution, and reproduction in any medium, provided the original work is properly cited.

In this context, Lu & Likos (2004) recognize that some rational way of predicting the extent of the wetting/drying process must be used, defining the contours to obtain the most appropriate SWCC. Due to practical limitations, it is common to model the drying SWCC as representative of the process in general (Lu & Likos, 2004). Leong & Rahardjo (1997) say that drying curves provide higher permeability coefficients and, consequently, more conservative Factor of Safety (*FoS*). Zhai et al. (2016) and Kristo et al. (2019) reached the same conclusions, although they argue about the need to investigate the role of SWCC hysteresis in seepages.

Nevertheless, such an approach is not very simple. According to Lu & Likos (2004) and Fredlund et al. (2012), the wetting path of the retention curve is often ignored because adsorption curves are the hardest to evaluate. In the drying sector, the methodologies are standard, less complex, and most commonly measured. Chai & Gao (2021) add that determinations of wetting curves are not included in most laboratory test routines and that a possible approach would be to build them from other more easily determinable soil properties, such as the drying SWCC.

In this scenario, in which available techniques for direct measurements are limited, Likos et al. (2014) reveal that numerous models (physical and empirical) have been proposed for constructing curves in SWCC, both for main and for the scanning curves. Pham et al. (2005) reviewed physical and empirical hysteresis models applied to experimental data from 34 soils available in the literature. The authors concluded that the empirical model of Feng & Fredlund (1999) with improvements of Pham et al. (2003) provided the best predictions of main wetting curves. This model is simple, can be used to obtain any of the main SWCC curves and can also be used in conjunction with traditional fitting equations, such as Fredlund & Xing (1994). It is necessary experimental determination of one of them (drying or wetting) and two points on the other curve, points that can be estimated, as explained by Pham et al. (2003). Equation 1 represents the proposal.

$$w(\psi) = \frac{w_u \cdot b + c \cdot \psi^d}{b + \psi^d} \quad (1)$$

where w_u is the water content for suction equal to 0 or saturated water content, c is the water content for high suction or residual suction values, b is an adjustment parameter that determines the horizontal position of the curve, and d is a fit parameter that represents the slope of the inflection point of the curve.

Another important parameter is hydraulic conductivity, which is variable for unsaturated soils and can be considered as a function of volumetric moisture or suction. Fredlund et al. (2012) argue that the increase in matric suction decreases the volume of pores occupied by water, restricting its movement. Conductivity measurements for unsaturated soils can be direct or indirect. The direct ones are the field

or laboratory techniques. Indirect techniques are based on the soil retention curve and saturated permeability. With these, it is possible to estimate the permeability for different suction values. Fredlund et al. (1994) proposed a suction range from 0 to 10^6 kPa. By hypothesis, the structure of the soils does not change with the variation of suction. Equation 2 expresses the proposal:

$$k(\psi) = k_s \frac{\int_{\ln(\psi)}^b \frac{\theta(e^y) - \theta(\psi)}{e^y} \theta'(e^y) dy}{\int_{\ln(\psi_b)}^b \frac{\theta(e^y) - \theta_s}{e^y} \theta'(e^y) dy} \quad (2)$$

where $k(\psi)$ (m/s) is the permeability coefficient in suction ψ (kPa), k_s is the saturated permeability (m/s), θ is the volumetric water content (m^3/m^3), θ_s is the volumetric water content in saturated condition (m^3/m^3), e is the Euler's number, ψ is suction (kPa); ψ_b is the air entry value (kPa), b is $\ln(10^6)$, y is the integration variable that represents the logarithm of suction, and θ' is the first derivative of the SWCC proposed by Fredlund & Xing (1994).

In light of the previous brief exposition, a study of the stability of a residual soil slope in an unsaturated approach is presented. To circumvent a certain degree of uncertainty of the material, a parametric analysis was adopted. Therefore, it is possible to investigate the flow behaviour and stability of the slope in scenarios that involve material variability and rainfall characteristics, allowing a better understanding of how the various factors interfere with the soil response.

2. Materials and methods

2.1 Material

The study is a slope executed to allow the occupation of the land and the formation of transport infrastructure within the scope of a wind farm. It is located in the city of Pindaí, in Bahia, 805 km from Salvador. The main slope is composed by two secondary slopes. It has a considerable degree of homogeneity and an undisturbed cubic block of soil (50 cm × 50 cm) was extracted from slope's base, and treated as representative of the entire problem. The soil is residual and tropical. The aim is to verify the influence of hydraulic parameters and rainfall characteristics.

2.2 Laboratory tests performed

The characterization tests performed were the grain size analysis (ABNT, 2016a), determination of bulk density of undisturbed samples (ρ_b), field moisture (w_0), and void ratio (e_0) (ABNT, 2020), determination of the specific gravity of soil particles (γ_s) (DNER, 1994), and determination of the consistency limits (ABNT, 2016b, c). The results are summarized in Table 1.

The soil was classified as low compressibility clay by the Unified Soil Classification System (CL) and as A6 by the AASHTO Classification System.

The hydraulic properties tests were the determination of saturated hydraulic conductivity (ABNT, 2021) and the determination of the retention curve by the filter paper technique (ASTM, 2016). The filter paper type was Whatman n° 42 185 mm and calibration curve was the Chandler & Gutierrez (1986)'s proposal. The Fredlund and Xing's (1994) unimodal model was used for the adjustment curve of matric suction of paper filters in function of gravimetric moisture of samples. The observed matric suction interval was from 0 to 10,000 kPa.

For the strength parameters, the tests were the consolidated undrained triaxial compression test for the effective parameters of the Mohr – Coulomb criterion (ϕ' and c') and the direct shear test to determine the unsaturated shear strength parameter (ϕ^b). The parameter ϕ^b originates from the model proposed by Fredlund et al. (1978), representing the increase in shear strength due to suction. Therefore, it is necessary a suction control of the tested samples. To achieve this requirement, a conventional direct shear equipment was used (ASTM, 2011), with known moisture samples and estimated suction by the retention curve. The results obtained were 24.9°, 12 kPa and 13.3°, for ϕ' , c' and ϕ^b , respectively.

2.3 Soil parameters analyzed

Saturated permeability and SWCC were chosen to be parameterized. The retention curves used were the main drying and wetting curves. Three values of saturated permeability were defined based on the result obtained experimentally.

The empirical model of Feng & Fredlund (1999) with improvements of Pham et al. (2003) was chosen to determine the main wetting SWCC from the drying SWCC determined in the laboratory. After constructing the wetting path, it is possible to represent the new curve in terms of the parameters of the Fredlund & Xing (1994) model. Figure 1 shows the wetting and drying curves. Table 2 summarizes the parameters of Fredlund & Xing (1994).

From Figure 1, since the experimental data curve presents a very discrete bimodal behaviour, the drying SWCC curve is satisfactorily modeled in a unimodal way by Fredlund & Xing's (1994) model. Bimodal represents a typical shape of tropical soils. Due to their formation process, these soils have structures with macro and micropores and a complexity of ions in their forming clay minerals. The desaturation of macropores and micropores can result in a retention curve with plateaus.

Defined in the laboratory stage, the saturated conductivity was 7.19×10^{-6} m/s (low permeability soil). This value refers to the extracted undisturbed block. Due to the variability of residual soil characteristics, saturated hydraulic conductivity may vary slightly for different portions of the slope. To include this variability, the values used in parametric analysis were 7.19×10^{-5} , 7.19×10^{-6} , and 7.19×10^{-7} m/s, the first and the

last differing by an order of magnitude from the experimental value. The hydraulic conductivity function was defined by the method presented by Fredlund et al. (1994) for the wetting and drying curves.

2.4 Study of precipitation

The rainfall characteristics were obtained from the National Water Agency (ANA) database. The investigated post is located in the city of Pindaí, Bahia. The location had data from 2005 to 2021. The data collected was used in two phases. The first phase corresponds to the determination of the initial suction profile, evaluating its behaviour throughout the year, and identifying its most critical conditions for the safety of the slope. The weekly rainfall distribution for 2009 was used, as it is the closest to the historical averages from 2005 to 2021. The second phase corresponds to the determination of scenarios to visualize the variation of the FoS as a function of time.

Table 1. Index properties and consistency limits.

ρ_b (g/cm ³)	1,7
e_0	0,65
w_0 (%)	3,76
γ_s (g/cm ³)	2,69
LL (%)	38
PL (%)	20

Legend: see List of Symbols and abbreviations.

Table 2. Fredlund & Xing (1994) parameters.

Parameters	Drying	Wetting
a	4.3	1.8
m	0.177	0.35
n	9.4	9
ψ_r (kPa)	7206	7206

Legend: see List of symbols and abbreviations.

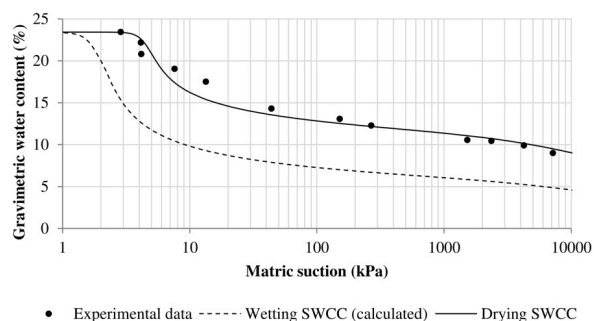


Figure 1. SWCC for drying and wetting paths.

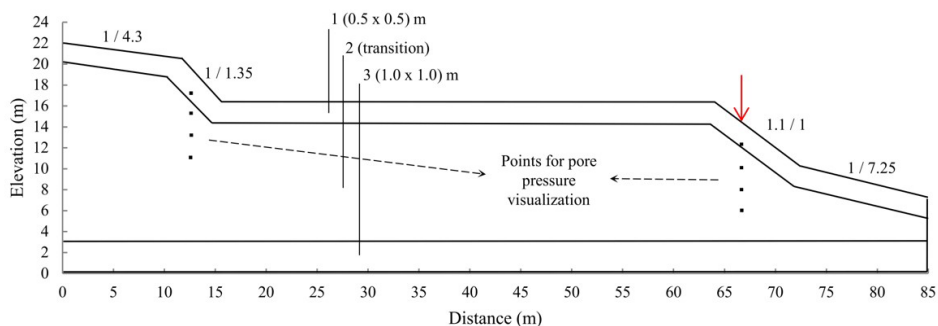


Figure 2. Slope mesh for seepage analysis.

Table 3. Rainfall scenarios for the second phase of seepage analysis.

Scenarios	Antecedent rainfalls				Main rainfalls			
	Total (mm)	Number of events	Duration/event (h)	Intensity (mm/h)	Total (mm)	Number of events	Duration/event (h)	Intensity (mm/h)
1	-	-	-	-	130	1	24	5.42
2	90	3	24	1.25	150	1	24	5.42
3	-	-	-	-	360	3	48	2,5
4	75	1	24	3.12	150	1	24	5.42

In this case, the three months in the historical series with the highest rainfall volumes were selected. These were December 2013, January 2016 and December 2021. They served as a starting point for defining the scenarios, which are summarized in Table 3.

The four scenarios for the second phase of the infiltration analysis (Table 3) are 31 days long, however not all of them correspond to precipitation. These are present in just a few days and this was a simplification that aimed to better visualize the recovery of strength due to matric suction, evaluated by the variation of FoS .

2.5 Seepage analysis

The software used was Seep/w 2023.1 (GEOSTUDIO International Ltd.), and the seepage analyzed was divided into two phases. The first corresponds to the definition of the initial suction profile, and the second to the application of the defined rainfall scenarios. Each one with its own boundary conditions applied to the modeled slope surface. In the sense of simplification, the slope is considered to be composed of homogeneous and isotropic residual soil. Six soil configurations were defined, combining the two retention curves and the three values of saturated conductivity, summarized in Table 4.

Regarding the slope geometry, from the upper point of the right border to the left border, the difference between the elevations is 15 meters high. From right to left, the horizontal angles are 7.85° , 47.59° , 36.56° and 13.06° . The elevation of the groundwater table was set at three meters above the lower boundary of the problem. Thus, it is 10 meters down from the

Table 4. Nomenclature of the soil configurations.

Saturated hydraulic conductivity	Retention curve - Drying	Retention curve - Wetting
k_{s1} (7.19×10^{-5} m/s)	RCD - k_{s1}	RCW - k_{s1}
k_{s2} (7.19×10^{-6} m/s)	RCD - k_{s2}	RCW - k_{s2}
k_{s3} (7.19×10^{-7} m/s)	RCD - k_{s3}	RCW - k_{s3}

Legend: see List of symbols and abbreviations.

midpoint of the face of the slope on the right, a value close to those found in works of the same nature, such as those by Kristo et al. (2019), Cai & Ugai (2004) and Tsaparas et al. (2002).

The finite element mesh was divided into three regions. The first comprised the surface to a depth of 2 meters and was intended for greater discretization to overcome convergence problems. The second was below region 1 up to 3 meters above the lower boundary of the problem, corresponding to an intermediate zone. Finally, the remaining domain was considered the third region, the lower border up to a height of 3 meters, intended for fixing the water level at an elevation of 3 meters. To region 1, rectangular elements measuring $0.5 \text{ m} \times 0.5 \text{ m}$ with eight nodes were assigned. Region 3 was discretized with $1.0 \text{ m} \times 1.0 \text{ m}$ elements with 4 nodes. Finally, for region 2 there were rectangular and triangular transition elements with 4 nodes, connecting the more and less refined meshes. Also, eight points were added for observing of pore pressure variations, as shown in Figure 2.

The boundary conditions common to both phases were infinite slope conditions along the left and right boundaries of the domain, preventing edge influences on the results, and zero

flow condition at the lower boundary nodes. The groundwater table was kept fixed at an elevation of three meters for the first phase. For the second phase, the water table was allowed to rise.

For the first phase of the analysis, a $\text{m}^3/\text{s}/\text{m}^2/\text{week}$ water flow function was modeled for 52 weeks (~ 1 year). The distribution of weekly rainfall for the year 2009 was chosen to compose the values of the function. At the end of 52 weeks, a new simulation with the same characteristics was performed, with the initial condition being the final pore water pressure profile of the first one. The same procedure was repeated several times until it was observed that the pore pressure results assumed a representative annual stationary regime. For the second phase of the analyses, four $\text{m}^3/\text{s}/\text{m}^2/\text{day}$ water flow functions were modeled for 31 days. Each function received the values corresponding to the four defined rainfall scenarios. The initial pore pressure profile of the second phase analysis is the most critical from the first.

2.6 Slope stability analysis

Slope stabilities under different conditions were evaluated using the Morgenstern-Price method for the second phase of seepage analysis. The software used was *Slope/w* 2021.4 (GEOSTUDIO International Ltd.). The geometry studied is composed of two secondary slopes, each of which was analyzed independently. Therefore, for the same day, there are two *FoS*, one for the left slope and one for the right.

3. Results and discussions

3.1 Initial suction profiles

A representative annual variation regime of pore water pressure was achieved in the fourth year (or fourth cycle) for all soil configurations, varying in points such as the extent of pore pressure changes and the temporal position of the situation most unfavorable to stability. It can be seen that the evolution of pore pressures is a function of the period of the year, whether drier or rainier. The rainy season is between the second half of October and the first of April, and the dry season is between the second half of April and the first of October. The water balance of the dry one relies only on the drainage mechanisms, without relevant rainfalls.

It is of fundamental interest to determine the most critical profiles (lowest suctions) to slope stability for the six soil configurations. The lowest suction situation means that the contribution of matric suction in the shear strength reaches the lowest level, and the action of the weight of retained rainwater in the soil in the increase of the requesting forces is maximum. The profiles were defined as vertical lines starting from the lower boundary of the problem and passing through the eight representative points on both the left and right sides. As the right points proved to be more critical, the discussion about the profiles was based on the presentation of their results only. Therefore, all

suction and saturation degree profiles in the following figures are related to the imaginary vertical line below the red arrow in Figure 2. Figures 3 and 4 show the results for SWCC in the drying and wetting paths. Z (m) represents the depth from the lower boundary of the problem. The dashed horizontal line represents the water table. The inclined line represents the water pore pressures varying linearly in the saturated region: positive in the zone below the water table and negative in the capillary fringe, from which the soil becomes unsaturated. Three curves branch from the inclined straight line and represent the pore pressure variation above the capillary fringe.

The critical hydraulic conductivity profiles of $\text{RCD} - k_{s1}$ and $\text{RCW} - k_{s1}$ are found at the end of the 44th week of the year (the beginning of November). For the other configurations, the profiles were reached in the 15th week (the second half of April). The critical profiles for the hydraulic conductivity of 10^{-6} and 10^{-7} m/s (k_{s2} and k_{s3}) are associated with the wet season, as they occur at the end of it. Different from the profiles for the hydraulic conductivity of 10^{-5} m/s, these seem to be linked to a specific event, not to the entire rainy season.

The year used as representative (2009) has events with an order of magnitude that does not exceed 10^{-7} m/s. A conductivity of 10^{-5} m/s seems to prevent the slope from suffering an

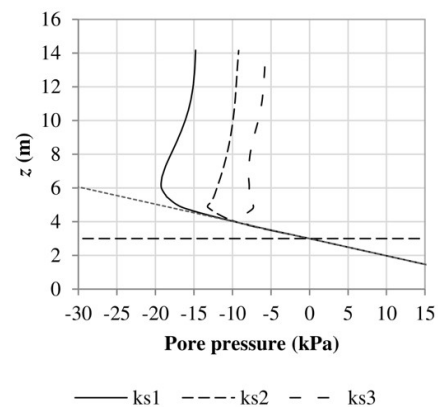


Figure 3. Critical suction profiles for drying SWCC configurations.

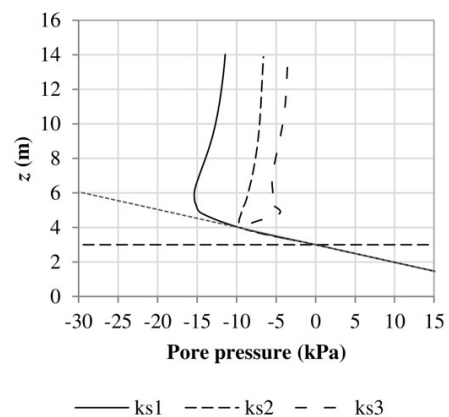


Figure 4. Critical suction profiles for wetting SWCC configurations.

accumulative effect of rainwater in the long term, as the drainage conditions are quite favorable. Thus, it is coherent that the most unfavorable moment for stability is the one immediately after a specific event (extreme or sequence thereof), with pore water pressures decreasing again soon after. Figures 3 and 4 show that the wetting curve leads to more unfavorable profiles for stability than the drying curve for all k_s values.

3.2 Responses to the rainfall scenarios

The discussions in this item are not extended to the monthly rain scenarios in their entirety, but focus only on a few events for a more objective understanding. For the configurations $RCD - k_{s1}$ and $RCD - k_{s3}$ (see Table 4), the pore water pressure profiles were analyzed for the end of day 1 of scenario 1 and the end of day 2 of scenario 3, corresponding to a rainfall of 130 mm in 24h and a rainfall of 120 mm in 48h, respectively. In this way, the precipitated volumes were close, but with different durations. The results for $RCD - k_{s1}$ are shown in Figure 5. For similar volumes, it is possible to see that the wetting front of a longer-duration event has more potential to influence the pore pressures within the slope.

The most intense event (relationship between precipitated volume and its duration) produces the greatest pore pressures on the surface compared to the least intense. However, for certain more internal points, as for the depth of 6 meters, the least intense event causes the greatest pore pressures. For the $RCD - k_{s3}$ configuration, the most intense event also produces the largest pore pressures on the surface; however, for the more internal points, the duration seems irrelevant. This is shown in Figure 6.

For $RCD - k_{s1}$, the two precipitation intensities are lower than k_{s1} , so the slope does not reach a zero pressure condition at the surface (Figure 5). About k_{s3} , there is a higher and lower intensity. Consequently, the soil is superficially saturated for the event of higher intensity (Figure 6). This saturated surface layer works as a barrier to the advance of the wetting front, not allowing it to reach more internal regions. Consequently, in real situations, a posterior volume precipitating on the slope cannot infiltrate, eventually forming a surface runoff. Although this barrier does not exist for k_{s1} , a portion of the flow that travels through the surface and does not infiltrate also exists, albeit to a lesser extent. It is more prominent for more intense events, resulting in a more negligible infiltration.

For the configurations $RCD - k_{s1}$ and $RCD - k_{s3}$, Figures 7 and 8 present the degree of saturation for the events represented in Figures 5 and 6. It shows the innermost points with higher water content under less intense precipitation for $RCD - k_{s1}$ (see Figure 7) and the occurrence of surface saturation under the most intense event for $RCD - k_{s3}$ (see Figure 8).

For the drying curve, comments were limited to configurations with hydraulic conductivities k_{s1} and k_{s3} , as k_{s2} provides intermediate results. For the same permeabilities and events, the results for the wetting SWCC show less negative pore pressures and saturation degrees closer to 1, as

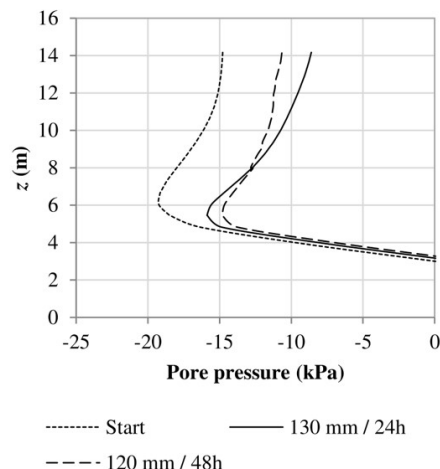


Figure 5. Suction profiles for $RCD - k_{s1}$ after selected events.

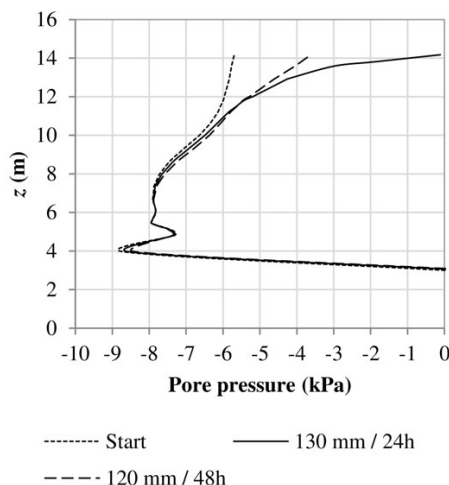


Figure 6. Suction profiles for $RCD - k_{s3}$ after selected events.

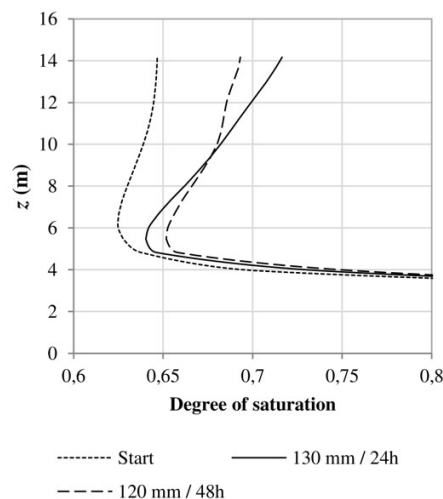


Figure 7. Degrees of saturation for $RCD - k_{s1}$.

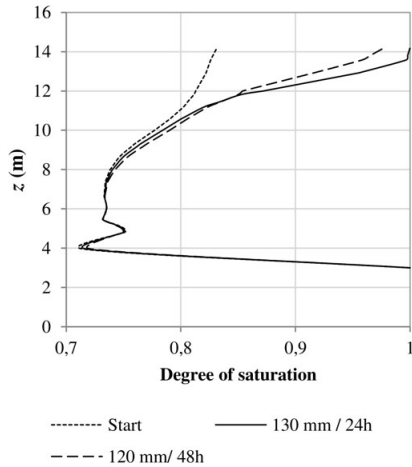


Figure 8. Degrees of saturation for RCD – k_{s3} .

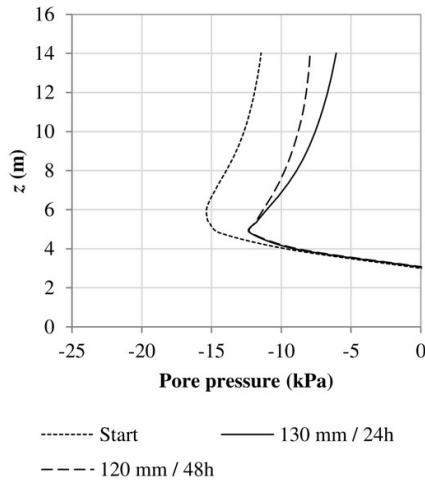


Figure 9. Suction profiles for RCW – k_{sl} after selected events.

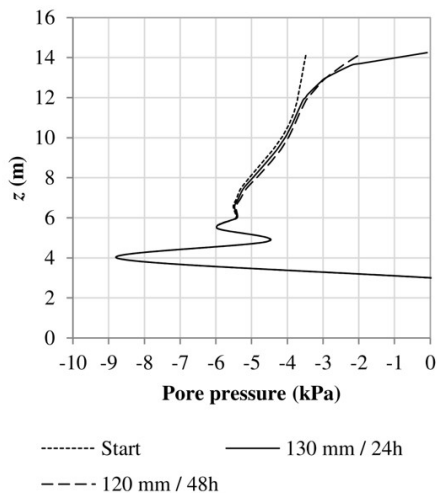


Figure 10. Suction profiles for RCW – k_{s3} after selected events.

shown in Figures 9 and 10, for the RCW – k_{sl} and RCW – k_{s3} configurations, respectively.

Differently from what happened for RCD – k_{s1} , the less intense event did not advance as deeply, not overcoming the pore pressures obtained by the more intense event. Therefore, for this saturated conductivity, when comparing the two retention curves, there is a visible change in the behaviour of the wetting front.

From Figures 6 and 10, for k_{s3} , the responses for the drying and wetting curves are pretty close, except for the fact that the latter provides a smaller reach of the wetting front. Because of the presented comments, for higher saturated conductivities or conductivities higher than the intensities of the rainfall events, it emerges that the option for the study of pore water pressures by a drying or wetting curve can be significant. Otherwise, a choice between them may not be relevant.

3.3 Slope stability analysis

Again, the discussions in this item are not entirely extended to the rainfall scenarios but focus only on a few events for objectivity. Scenario 2 was used to compare the evolution of FoS for configurations with the same saturated conductivity but with different SWCC. This scenario was chosen, but the same trend was observed for the others. Figure 11 summarizes the results. The vertical dotted lines represent the rainfall events.

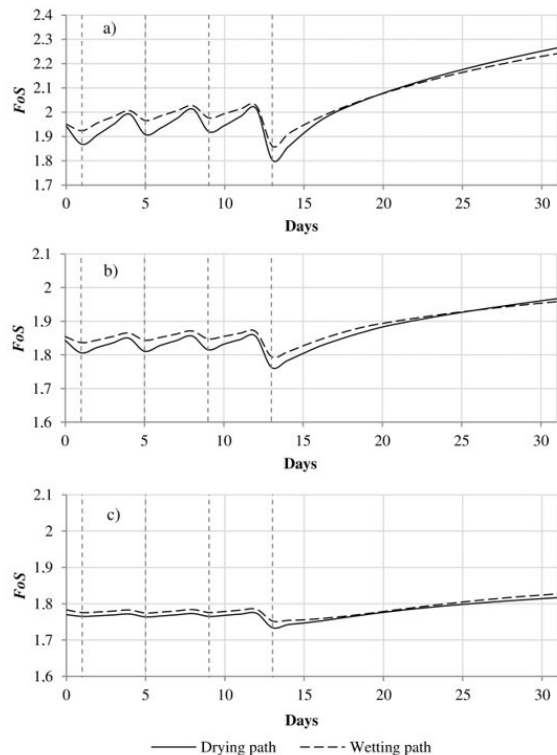


Figure 11. Results of scenario 2 for slope stability: (a) k_{sl} ; (b) k_{s2} ; (c) k_{s3} .

Figure 11 shows that the recovery of the FoS starts at the exact moment that the rainfalls end, regardless of the retention or permeability curve used. It is possible to identify that the values of FoS derived from the drying curves are more conservative for most of the time considered. They are also the ones that are reduced and recovered more quickly. It is even possible to notice the FoS of the drying SWCC surpassing those of the wetting SWCC sometime between days 20 and 25 for conductivities k_{s1} and k_{s2} . Although the drying curve produces a more significant variation than the wetting curve, this characteristic is also a function of the saturated permeability. The results referring to the highest saturated permeability (k_{s1}) show a more pronounced reduction and recovery of the FoS compared to the other conductivities. For the smallest one (k_{s3}), the variations in FoS are minimal, with the wetting and drying curves appearing very close and almost coincident, although the latter is always more conservative.

From the late observation for the lowest permeability (k_{s3}), it emerges that this permeability restricts the action of rainfall in promoting significant reductions in the FoS . Therefore, a very low permeability practically eliminates the difference between the results of the drying and wetting curves, making the choice between them irrelevant.

Such behaviours find justification in the hysteresis of the hydraulic conductivity function. For the same matric suction, wetting curves correspond to lower permeabilities than drying ones. As a result, water takes longer to reach deeper soil layers. The use of the drying curve allows the water to infiltrate faster and deeper, reducing the matric suction and the portion of the shear resistance due to it. It also allows the water to be drained through the layers more quickly, causing a faster increase in matric suctions and recovery of the FoS . Similar findings can be found in the works of Tsaparas et al. (2002), Cai & Ugai (2004) and Kristo et al. (2019). The latter obtained curves close to those shown in Figure 11. This fact is more visible for higher permeabilities and less relevant for smaller ones.

Figure 12 shows the results grouped by retention the curve for scenario 2. The lower the saturated hydraulic conductivity, the lower the FoS . However, the explanation for what happened is in the initial conditions and not strictly in the soil characteristics. The initial pore pressures obtained in the annual transient analyses for the configurations with k_{s3} are higher.

As illustrated in Figures 11 and 12, modeling by the wetting curve or by lower saturated conductivities causes a slower reduction and recovery of the FoS , which may be less conservative than the results for drying curves or higher conductivities. However, such behaviour is also influenced by the intensity and duration of rainfalls.

For events of long duration and intensity lower than the saturated hydraulic conductivity, the FoS tends to decay faster at the beginning and stabilize during the event. In this case, the redistribution of water within the slope has come into equilibrium, and the FoS no longer changes in the remaining time of the event (or at least until the groundwater-table starts to rise). On the other hand, for events of long duration and

intensity greater than the hydraulic conductivity, the FoS tends to decrease more slowly than in the first case for the rainfall onset. However, it tends to accelerate its decrease over time, surpassing the rate of change of the FoS for the first case. In this situation, the redistribution flow does not reach equilibrium until the slope is completely saturated.

In that view, it is established that part of the explanation of the behaviour of the FoS for the different configurations and scenarios presented is found in characteristics of precipitations. For faster FoS reductions and recoveries, hydraulic parameters are important, but not absolute.

The constitutive relationships used in this study and which configure two of the three hydraulic properties of the soil were the SWCC and the unsaturated hydraulic conductivity curve (Equation 2). They were obtained by the traditional methodology of applying a sequence of hydrostatic equilibrium states from the gradual drainage of an initially saturated soil sample with the determination of the respective humidity at the end of equilibrium. It was assumed that these constitutive relationships encompass all processes and effects that control water movement in the soil, such as surface tension, wettability of solid surfaces, shape and interconnection of the conducting pores. This assumption results in a uniqueness relationship between water content and pore pressure. However, this does not match reality. The relationship between moisture and pore pressure in transient flow is not unique and is controlled by a range of factors such as relaxation of the air-water interface, dissolution of trapped air, temporal changes in wettability, among others, which are not yet fully explored. This phenomenon is known as dynamic nonequilibrium (DNE) of water flow in porous media (Diamantopoulos & Durner, 2012).

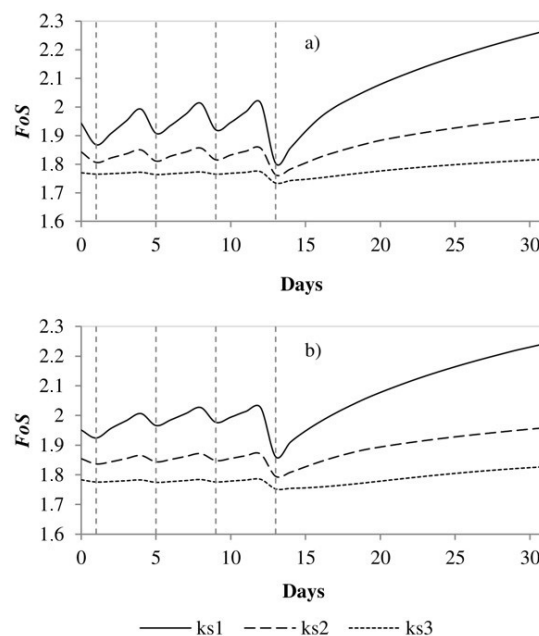


Figure 12. FoS by SWCC for scenario 2: (a) drying path; (b) wetting path.

The standard Richards equation is used in this study to model water flow in the vadose and saturated zones of the slope. However, DNE effects are not covered by it and this represents the central limitation of this numerical analysis.

4. Conclusions

During the 31 days of analysis, for all scenarios and configurations, SWCC in the drying path produced greater variations in the FoS , with faster reductions and recoveries, when compared to the responses of the wetting curves. However, the influence of using different trajectories, the amplitude of variation, and the speed of changes were related to saturated permeability. The highest value of this parameter showed a more pronounced difference in behaviour between the retention curves. For the lowest conductivity, it was not possible to identify sensitive differences.

The drying curves also resulted in more conservative values of FoS during most of the analysis time. Depending on the combination of parameters and the scenario, it was possible to observe the FoS of the drying SWCC overcoming those of the wetting curve at some point. This happened for the configurations of higher and intermediate saturated conductivity (k_{s1} and k_{s2}). Regarding the configurations with the lowest saturated permeability value, the FoS of the drying SWCC were always more conservative than those of the wetting path.

The above behaviour is in agreement with the results for pore water pressures, as a faster increase and decrease in pore pressures lead to faster losses and gains in shear strength due to matric suction, reflecting on the FoS . Results aligned with previous works, such as Kristo et al. (2019) and Tsaparas et al. (2002), indicating the critical role of SWCC and saturated hydraulic conductivities on seepage and stability assessments.

For the considered rainfalls, the advance of the wetting front is a function of the retention curve and saturated permeabilities. For higher permeabilities, the deeper the wetting front, with the drying curve providing a slightly greater advance than the wetting curve. For the lowest permeabilities, the front is more superficial and the difference between the retention curves is little noticeable. When considering isolated events, for the combination of the drying curve with the highest saturated permeability, more distributed events showed greater advancement of the wetting front than more intense events. For the other configurations, this fact was not observed. Especially for those with the lowest saturated conductivity value, different intensities resulted in very similar pore pressure profiles, indicating a leading role of hydraulic parameters in water redistribution patterns.

There is an indication that the use of drying or wetting retention curve in modeling is a more decisive choice in soils with greater saturated permeability, being of little influence on the responses for more impermeable soils.

The conclusions of the numerical analysis were obtained without considering the effects of nonequilibrium effects in SWCC and hydraulic conductivity functions. However, the conclusions contribute to a better general understanding of

the impact of studied parameters on the strength and FoS of unsaturated soils.

Acknowledgements

The authors would like to thank Brazilian National Council for Scientific and Technological Development (CNPq) and Federal University of Ceará for supporting the research activities described in this paper.

Declaration of interest

The authors have no conflicts of interest to declare. All co-authors have observed and affirmed the contents of the paper and there is no financial interest to report.

Authors' contributions

Jorge Henrique Ribeiro Lins: conceptualization, data curation, visualization, writing – original draft. Francisco Chagas da Silva Filho: conceptualization, data curation, methodology, supervision, validation.

Data availability

The datasets produced and analyzed in the course of the present study are not public but may be available from the corresponding author on reasonable request.

List of symbols and abbreviations

<i>a</i>	Fredlund & Xing (1994) Coefficient
<i>b</i>	Feng & Fredlund (1999) Coefficient; Fredlund et al (1994) Coefficient
<i>c</i>	Feng & Fredlund (1999) Coefficient
<i>c'</i>	Effective cohesion of Mohr-Coulomb failure criteria
<i>d</i>	Feng & Fredlund (1999) Coefficient
<i>e</i>	Euler's number
<i>e₀</i>	Field void ratio
<i>k</i>	Hydraulic conductivity of soil
<i>k_s</i>	Saturated hydraulic conductivity of soil
<i>m</i>	Fredlund & Xing (1994) Coefficient
<i>n</i>	Fredlund & Xing (1994) Coefficient
AASHTO	American Association of State Highway and Transportation Officials
ANA	National Water Agency
CL	Low compressibility clay
DNE	Dynamic nonequilibrium
<i>FoS</i>	Factor of Safety
<i>LL</i>	Liquid limit
<i>PL</i>	Plastic limit
RCD	Retention curve - Drying
RCW	Retention curve - Wetting
<i>S</i>	Degree of saturation

$SWCC$	Soil water characteristic curve
w	Gravimetric water content
w_u	Saturated water content for Feng & Fredlund (1999) proposal
w_0	Field water gravimetric content
y	Fredlund et al. (1994) Coefficient
z	Depth from lower boundary of the problem
ϕ'	Effective friction angle of Mohr-Coulomb failure criteria
ϕ^b	Unsaturated shear strength parameter
γ_s	Specific gravity of soil particles
θ	Volumetric water content
θ_s	Saturated volumetric water content
θ^{\prime}	First derivative of Fredlund & Xing's (1994) equation.
ρ_b	Bulk density of undisturbed samples
ϕ^*	Effective friction angle of Mohr-Coulomb failure criteria
ϕ^b	Unsaturated shear strength parameter
ψ	Suction
ψ_b	Air entry value
ψ_r	Residual suction

References

- ABNT NBR 7181. (2016a). *Soil: grain size analysis*. Associação Brasileira de Normas Técnicas, Rio de Janeiro.
- ABNT NBR 6459. (2016b). *Soil: liquid limit determination*. Associação Brasileira de Normas Técnicas, Rio de Janeiro.
- ABNT NBR 7180. (2016c). *Soil: plasticity limit determination*. Associação Brasileira de Normas Técnicas, Rio de Janeiro.
- ABNT NBR 16867. (2020). *Soil: determination of the bulk density of undisturbed samples: method using hydrostatic weighing*. Associação Brasileira de Normas Técnicas, Rio de Janeiro.
- ABNT NBR 14545. (2021). *Soil: determination of the permeability coefficient of clay soils at variable load*. Associação Brasileira de Normas Técnicas, Rio de Janeiro.
- ASTM D3080-11. (2011). *Standard test method for direct shear test of soils under consolidated drained conditions*. ASTM International, West Conshohocken, PA. http://dx.doi.org/10.1520/D3080_D3080M-11.
- ASTM D5298-16. (2016). *Standard test method for measurement of soil potential (suction) using filter paper*. ASTM International, West Conshohocken, PA. <http://dx.doi.org/10.1520/D5298-16>.
- Cai, F., & Ugai, K. (2004). Numerical analysis of rainfall effects on slope stability. *International Journal of Geomechanics*, 4(2), 69-78. [http://dx.doi.org/10.1061/\(ASCE\)1532-3641\(2004\)4:2\(69\)](http://dx.doi.org/10.1061/(ASCE)1532-3641(2004)4:2(69)).
- Chai, J., & Gao, Z. (2021). Method for predicting drying-wetting and scanning soil-water characteristic curves. *Transportation Geotechnics*, 31, 100666. <http://dx.doi.org/10.1016/j.trgeo.2021.100666>.
- Chandler, R.J., & Gutierrez, C.I. (1986). The filter-paper method of suction measurement. *Geotechnique*, 36(2), 265-268. <http://dx.doi.org/10.1680/geot.1986.36.2.265>.
- Carvalho, J.C., Gitirana Junior, G.F.N., Machado, S.L., Mascarenha, M.M.A., & Silva Filho, F.C. (2015). *Solos não saturados no contexto geotécnico* (1ª ed., Vol. 1). São Paulo: Associação Brasileira de Mecânica dos Solos e Engenharia Geotécnica.
- Diamantopoulos, E., & Durner, W. (2012). Dynamic nonequilibrium of water flow in porous media: a review. *Vadose Zone Journal*, 11(3), vzj2011.0197. <http://dx.doi.org/10.2136/vzj2011.0197>.
- DNER ME 093. (1994). *Soil: determination of the specific gravity of soil particles*. Departamento Nacional de Estradas de Rodagem, Brasília.
- Feng, M., & Fredlund, D.G. 1999. Hysteretic influence associated with thermal conductivity sensor measurements. In *Proceedings from Theory to Practice of Unsaturated Soil Mechanics in Association with the 52nd Canadian Geotechnical Conference and the Unsaturated Soil Group* (pp. 14:2:14-14:2:20), Regina, Saskatchewan, Canada. Regina, Sask.: Canadian Geotechnical Society.
- Fredlund, D.G., & Xing, A. (1994). Equations for the soil-water characteristic curve. *Canadian Geotechnical Journal*, 31(4), 521-532. <http://dx.doi.org/10.1139/t94-061>.
- Fredlund, D.G., Xing, A., & Huang, S. (1994). Predicting the permeability function for unsaturated soils using the soil-water characteristic curve. *Canadian Geotechnical Journal*, 31(4), 533-546. <http://dx.doi.org/10.1139/t94-062>.
- Fredlund, D.G., Morgenstern, N.R., & Widger, R.A. (1978). The shear strength of unsaturated soils. *Canadian Geotechnical Journal*, 15(3), 313-321. <http://dx.doi.org/10.1139/t78-029>.
- Fredlund, D.G., Rahardjo, H., & Fredlund, M.D. (2012). *Unsaturated soil mechanics in engineering practice* (Vol. 926). New York: John Wiley & Sons. <http://dx.doi.org/10.1002/9781118280492>.
- Kristo, C., Rahardjo, H., & Satyanaga, A. (2019). Effect of hysteresis on the stability of residual soil slope. *International Soil and Water Conservation Research*, 7(3), 226-238. <http://dx.doi.org/10.1016/j.iswcr.2019.05.003>.
- Lai, C.H. (2004). *Experimental study of stress-dependent soil-water characteristics and their applications on numerical analysis of slope stability* [Doctoral dissertation, Hong Kong University of Science and Technology]. HKUST's repository. Retrieved in November 22, 2022, from <https://repository.ust.hk/ir/Record/1783.1-4162>
- Leong, E.C., & Rahardjo, H. (1997). Permeability function for unsaturated soils. *Journal of Geotechnical and Geoenvironmental Engineering*, 123(12), 1118-1126. [http://dx.doi.org/10.1061/\(ASCE\)1090-0241\(1997\)123:12\(1118\)](http://dx.doi.org/10.1061/(ASCE)1090-0241(1997)123:12(1118)).
- Likos, W.J., Lu, N., & Godt, J.W. (2014). Hysteresis and uncertainty in soil water-retention curve parameters. *Journal of Geotechnical and Geoenvironmental Engineering*, 140(4), 04013050. [http://dx.doi.org/10.1061/\(ASCE\)GT.1943-5606.0001071](http://dx.doi.org/10.1061/(ASCE)GT.1943-5606.0001071).
- Lu, N., & Likos, W.J. (2004). *Unsaturated soil mechanics*. New York: John Wiley.

- Pham, Q.H., Fredlund, D.G., & Barbour, S.L. (2003). A practical hysteresis model for the soil-water characteristic curve for soils with negligible volume change. *Geotechnique*, 53(2), 293-298. <http://dx.doi.org/10.1680/geot.2003.53.2.293>.
- Pham, H.Q., Fredlund, D.G., & Barbour, S.L. (2005). A study of hysteresis models for soil-water characteristic curves. *Canadian Geotechnical Journal*, 42(6), 1548-1568. <http://dx.doi.org/10.1139/t05-071>.
- Rahardjo, H., Satyanaga, A., Leong, E.C., Ng, Y.S., & Pang, H.T.C. (2012). Variability of residual soil properties. *Engineering Geology*, 141-142, 124-140. <http://dx.doi.org/10.1016/j.enggeo.2012.05.009>.
- Tsaparas, I., Rahardjo, H., Toll, D.G., & Leong, E.C. (2002). Controlling parameters for rainfall-induced landslides. *Computers and Geotechnics*, 29(1), 1-27. [http://dx.doi.org/10.1016/S0266-352X\(01\)00019-2](http://dx.doi.org/10.1016/S0266-352X(01)00019-2).
- Wesley, L.D. (1990). Influence of structure and composition on residual soils. *Journal of Geotechnical Engineering*, 116(4), 589-603. [http://dx.doi.org/10.1061/\(ASCE\)0733-9410\(1990\)116:4\(589\)](http://dx.doi.org/10.1061/(ASCE)0733-9410(1990)116:4(589)).
- Zhai, Q., Rahardjo, H., & Satyanaga, A. (2016). Variability in unsaturated hydraulic properties of residual soil in Singapore. *Engineering Geology*, 209, 21-29. <http://dx.doi.org/10.1016/j.enggeo.2016.04.034>.